SCIENCE CHINA Materials

ARTICLES

mater.scichina.com link.springer.com

Published online 13 December 2016 | doi: 10.1007/s40843-016-5139-y
Sci China Mater 2017, 60(1): 57–67

Nanomagnetic CoPt truncated octahedrons: facile synthesis, superior electrocatalytic activity and stability for methanol oxidation

Tianyu Xia[1,2,3], Jialong Liu[2], Shouguo Wang[1,3*], Chao Wang[3], Young Sun[3] and Rongming Wang[1,2*]

ABSTRACT Nanomagnetic CoPt truncated octahedral nanoparticles (TONPs) were successfully synthesised through a facile one-pot strategy. These single crystal CoPt TONPs with an average size of about 8 nm exhibit excellent electrocatalytic performance of both activity and stability for methanol oxidation reaction (MOR). The mass and specific activities of CoPt TONPs is 8 and 6 times higher than that of standard commercial Pt/C, respectively. After accelerated durability test (ADT), the loss of electrochemical surface area (ECSA) for CoPt TONPs is only 18.5%, which is significantly less than that of commercial Pt/C (68.2%), indicating that CoPt TONPs possess much better stability than commercial Pt/C in the prolonged operation. The Curie temperature of CoPt TONPs down to 8 nm is as high as 350 K with weak ferromagntism at room temperature (RT), which is greatly valuable for recycling in the eletrocatalytic applications.

Keywords: truncated octahedral nanoparticles, methanol oxidation reaction (MOR), accelerated durability test (ADT), ferromagntism

INTRODUCTION

The high cost and poor durability of Pt nanoparticles (NPs) prevent direct methanol fuel cells (DMFCs) from being scaled-up for commercial applications [1–3]. One of the most promising strategies is the introduction of non-precious 3d transition metals to form MPt bimetallic electrocatalysts (M=Fe, Co, and Ni) [4–7]. These MPt electrocatalysts with different shapes are proved to be a potential route for mitigating the cost as well as enhancing their catalytic performance [8,9]. This enhancement was attributed to the lattice contraction and downshift of the d-band center of Pt in the bimetallic structures [10].

Among various MPt alloys for the electrocatalytic application, CoPt bimetallic NPs have gained much attention because of its higher activity, stability, CO tolerance, and lower cost than pure Pt catalysts and even other MPt bimetallic materials (such as NiPt, FePt) [11,12]. For examples, CoPt networks show high specific activity in both methanol oxidation reaction (MOR) and formic acid oxidation (FAO) [13]. Dealloyed CoPt hollow nanowires with ultrathin wall exhibit well-preserved activities after 10,000 cycles [14]. The deposition of mesoporous Pt skin onto Co nanochains grants them high activity and superior CO tolerance in the MOR together with only a 20.2% loss of the Pt electrochemical surface area (ECSA) after a harsh durability test [15].

Apart from elemental composition, the size and shape also play an effective role in the electrocatalytic performance [16,17]. The catalyst surface with a nano-segregated Pt (111) skin structure was used to account vitally for the dramatic enhancement [18,19]. Due to the close-packed arrangement of surface atoms, octahedral and truncated octahedral MPt NPs equipped with index facets of {111} are stable in electrochemical conditions [19]. Therefore, CoPt NPs with the structure of octahedron or truncated octahedron have great possibility to exhibit excellent electrocatalytic activity and stability.

It has been well known that magnetic CoPt materials including CoPt NPs and thin films have a broad range of applications in recording media [20,21] and magnetic sensor [22]. Therefore, CoPt NPs are a good candidate to investigate the relationship between the magnetism and catalysis. Due to their intrinsic magnetic properties, the

[1] University of Science and Technology Beijing, Beijing 100083, China
[2] Department of Physics, Beihang University, Beijing 100191, China
[3] State Key Laboratory of Magnetism, Institute of Physics, Chinese Academy of Sciences (CAS), Beijing 100190, China
* Corresponding authors (emails: sgwang@ustb.edu.cn (Wang S); rmwang@ustb.edu.cn (Wang R))

addition of magnetic element provides an easy and quick way to recycle catalysts. For recycling, the synthesised materials should show ferromagnetism at room temperature (RT). The structure, size, shape together with composition of magnetic NPs dominate magnetic transition temperature [23]. For example, in our previous work [24], the Curie temperature of hollow FePt nanochains is 200 K for the size of 300 nm and is increased to higher than 390 K for 20 nm nanochains. The results from Sun's group [25] show that the superparamagnetic blocking temperature of 9.5 nm CoPt NPs increases from 105 to 205 K with increasing Co content from 37% to 69%, indicating the superparamagnetism for CoPt NPs at RT. Obviously, the Curie temperature of the designed CoPt NPs for electrocatalyst should be well manipulated for recycling after electrocatalytic reaction. That is to say, it is better for CoPt NPs to show ferromagnetism at RT.

In this work, a facile one-pot approach has been developed to synthesize CoPt truncated octahedral nanoparticles (TONPs) with near-monodispersity. The morphologies, crystalline phase, chemical states and compositions of CoPt TONPs were analysed. The electrocatalytic performances were investigated by cyclic voltammetry (CV) and linear sweep voltammetry (LSV). Remarkably, the mass activity of CoPt TONPs is greatly enhanced due to better tolerance to the intermediate poisoning species, where it reaches 2.4 A mg_{Pt}^{-1} but only 0.3 A mg_{Pt}^{-1} for standard commercial Pt/C catalysts for MOR. Furthermore, the magnetic properties were studied by a superconducting quantum interference device (SQUID) and super high resolution electron spin resonance (ESR), where the ferromagnetism at RT was confirmed.

EXPERIMENTAL SECTION

Chemicals and materials

Cobalt(III) acetylacetonate [$Co(acac)_3$], platinum(II) acetylacetonate [$Pt(acac)_2$], commercial Pt/C (40 wt.% Pt) catalyst were purchased from Alfa Aesar. Dimethylformamid (DMF), poly(vinylpyrrolidone) (PVP) (K-30, AR), methanol (CH_3OH), sulfuric acid (H_2SO_4), anhydrous ethanol and acetone were purchased from Chinese reagent companies. All reagents were analytic grade and used without further purification.

Synthesis of CoPt TONPs

In a typical synthesis, 20 mg $Co(acac)_3$, 28 mg $Pt(acac)_2$ and 70 mg PVP were dissolved in 20 mL DMF. After ultrasonication for 30 min, the resultant homogeneous solution was transferred to a 25-mL Teflon-lined stainless-steel autoclave. The sealed vessel was then heated to 180°C and maintained for 12 h before it was cooled to RT. The black NPs were collected by centrifugation, and further cleaned by anhydrous ethanol and acetone several times.

Characterization

The structure was characterized by a JEOL-2100F transmission electron microscope (TEM). TEM samples were prepared by dispersing the as-synthesised powders in ethanol with ultrasonic treatment, and then a solution was dropped on a Cu grid coated with porous carbon film. X-ray diffraction (XRD) patterns were detected using Rigaku D/max-2400 X-ray diffractometer with a Cu Kα X-ray sources (λ=0.15405 nm). The chemical compositions of the products were characterized via a Hitachi S-4800 scanning electron microscope (SEM) with an energy dispersive X-ray spectroscope (EDS), and PerkinElmer Optima 7000DV inductively coupled plasma optical emission spectrometer (ICP-OES). X-ray photoelectron spectroscopy (XPS) was performed on an ESCALAB 250Xi system.

Electrochemical measurements

The electrochemical measurements were conducted on a CH Instruments 660D electrochemical workstation at RT with a three electrode configuration. The working electrode was a glassy carbon electrode (the geometric area was 0.071 cm^2). The counter electrode and reference electrode was Pt wire and saturated calomel electrode (SCE), respectively.

To prepare the working electrode, 6 mg CoPt TONPs and 9 mg Vulcan XC-72 carbon were dissolved in 4 mL ethanol and ultrasonicated for 30 min. Then 5 μL of the suspension and 5 μL of 0.1% nafion solution, in turn, were dropped onto the working electrode surface and naturally dried in air. To compare the catalytic behavior, samples including other CoPt NPs and commercial Pt/C (not mixed with Vulcan XC-72 carbon) were prepared following the same process as CoPt TONPs.

Magnetic measurements

The magnetic properties of CoPt TONPs were measured via a SQUID magnetometer. Zero-field-cooled (ZFC) and field-cooled (FC) processes were carried out with an applied field of 100 Oe (1 Oe=0.012566 A m^{-1}). ESR measurement was carried out from 80 to 320 K using an ESR spectrometer (JEOL ESR FA-200) at X-band (9 GHz).

RESULTS AND DISSCUSSION

The morphologies of the as-prepared products were char-

acterized by TEM. As shown in Fig. 1a, the particles have truncated octahedral profile with an average size of about 8 nm. A narrow size distribution is shown by the inset in Fig. 1a. High-resolution TEM (HRTEM) image is shown in Fig. 1b, where *d*-spacing of the lattice is determined to be 2.11 and 1.85 Å, respectively. Those values are in good agreement with the (111) and (200) planes of the face-centered cubic (fcc) $CoPt_3$ alloy, respectively. Some steps can be clearly observed, where one step is marked by a blue arrow at the edge as an example. The lattice fringes of the whole particle are coherent, implying a single-crystal structure of the products. The selected-area electron diffraction pattern (SAED, shown in Fig. 1c) shows concentric rings with the index of (111), (200), (220), (311) and (222) planes, belonging to a typical fcc structure, in good agreement with the HRTEM image.

The powder XRD data of the TONPs are presented in Fig. 2a. It exhibits a typical pattern of an fcc structure. Peaks located at 40.5°, 47.1° and 68.8° can be ascribed to the corresponding (111), (200) and (220) planes, respectively, of an typical $CoPt_3$ fcc structure. In addition, no impurity peaks or mono-component Co and Pt peaks are found, verifying the formation of CoPt binary alloy. Fig. 2b is an SEM-EDS result of the sample, showing mainly Al, Si, Co and Pt characteristic peaks. Since the Al and Si come from the supporting Al substrate and Si wafer, it is confirmed that the product is composed of Co and Pt elements and the Co/Pt composition is about 1/3, in good agreement with the conclusion given by ICP-OES.

XPS analysis was used to characterize the chemical states of the CoPt TONPs shown in Figs 2c and d. The peaks located at 777.68 and 793.18 eV originate from metallic Co $2p_{3/2}$ and $2p_{1/2}$. Furthermore, two peaks located at 780.93 and 796.73 eV are clearly observed, indicating the presence of CoO because Co can be easily oxidized under ambient conditions [26,27]. The existence of shake up peaks of Co 2p is also caused by Co^{x+} $2p_{1/2}$. Similarly, two peaks located at 70.93 and 74.33 eV shown in Fig. 2d are derived from Pt $4f_{7/2}$ and Pt $4f_{5/2}$, while the corresponding standard value is 70.9 and 74.25 eV, respectively [28,29]. The two peaks can be split into two doublets, associated with Pt^0 and Pt^{2+} chemical states [30]. The existence of Pt^{2+} is assigned to the formation of PtO [1,31]. It is noteworthy that the binding energy of Pt peaks has a higher shift, quite probably owing to alloying of Co and Pt [32]. The XPS spectra can also be used to estimate the surface atomic ratio of elements [33], where the Pt fraction in surface is about 82.6%, higher than that of in bulk (75%) based on XRD, EDS and ICP. The

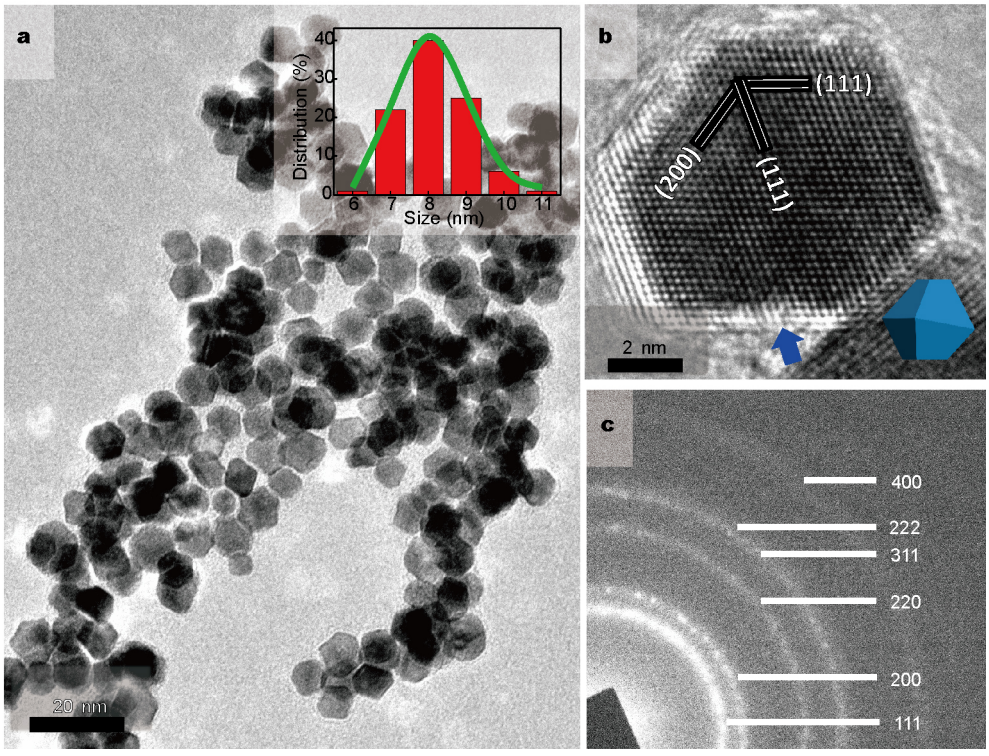

Figure 1 (a) Typical bright field TEM image and the corresponding size distribution (inset) of the as-prepared products; (b) HRTEM image and the corresponding geometric model (inset) of one CoPt NP, where a step is marked by blue arrow; (c) SAED pattern of (a).

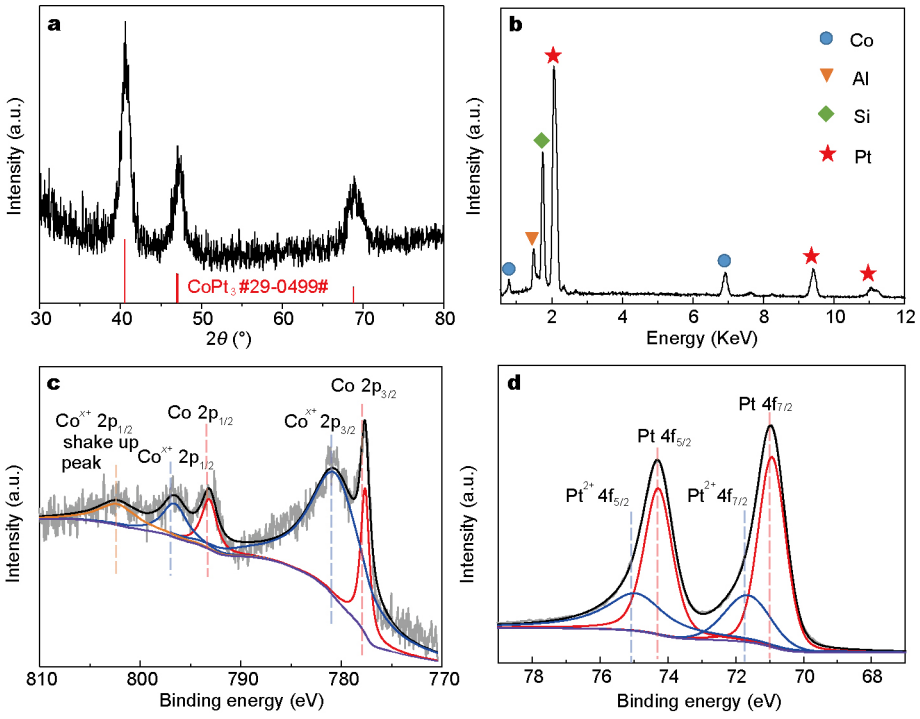

Figure 2 XRD (a) and EDS (b) patterns with 1:3 Co/Pt atomic ratio. High-resolution XPS spectra of Co 2p (c) and Pt 4f (d) in CoPt TONPs.

Pt-rich surface may be closely related with the electrocatalytic activity and stability, which will be discussed later in detail.

As previous work, for a long reaction time (16–42 h), DMF may play multiple roles, such as complexing agent, solvent, and reducing agent [34]. Long-time reaction, however, will not only waste a great deal of material resources, but also limit their wide industrial applications. Therefore, in this study, a short reaction time (such as 12 h) was tried and the influence of the reaction time on the products was interrogated. When the reaction time is decreased to 9 h with other conditions unchanged, the size of the as-prepared particles is smaller than that of normal CoPt TONPs (Fig. S1a, Supplementary information). With respect to the morphology, some particles show slightly concave edges while the others are similar to the CoPt TONPs. As shown in Fig. S1b, the particles become larger when the reaction time is extended to 15 h. The 15 h-particles show anomalous spherical structures with irregular boundaries. It is reasonable to conclude that the reaction time is an essential factor to control the well-defined truncated octahedral profile.

To gain further insight into the formation mechanism of CoPt TONPs, various amount and types of Co and Pt precursors were applied in the synthesis. As shown in Fig. S2a, with the increasing quantity of Co precursor, some small particles with the size about 2 nm are appeared. This is because excessive amounts of Co^{3+} are deoxidized into Co by DMF. By contrast, with the increase of Pt precursor quantity, some triangular structures are formed due to lack of deposition of Co atoms (Fig. S2b). Meanwhile, no matter replacing $Co(acac)_3$ by $CoCl_2{\cdot}6H_2O$ or replacing $Pt(acac)_2$ by K_2PtCl_6, uniform TONPs structure cannot be obtained which can be seen by TEM images (Fig. S3). These results provide direct evidence that the amount and kind of precursors can control the size and shape of the products.

Generally, NPs exhibit outstanding electrocatalytic performance, but it is easy for them to have aggregation. For ultrafine magnetic MPt alloys, with the increase of magnetism (Co >Fe >Ni) and decrease of NPs size, the issue of agglomeration becomes more serious. In order to overcome this disadvantage, it is necessary to develop an effective method to avoid aggregation. Fortunately, it has been found that PVP can be used to solve this problem very well [35]. In the parallel experiments with the absence of PVP, CoPt aggregated NPs (ANPs) were produced with non-uniform size and serious aggregation (Fig. S4), indicating that PVP served mainly as protecting and a dispersing agent for the products.

The ECSA is closely associated with the number of available active sites, where hydrogen adsorption/desorption peaks are typically used to evaluate the ECSA of catalyst

[36,37]. For comparison, CoPt TONPs, CoPt ANPs and commercial Pt/C electrocatalysts were investigated. Fig. 3a shows the CV curves of the above three catalysts in Ar-saturated 0.5 mol L^{-1} H_2SO_4 at a scan rate of 50 mV s^{-1}. It clearly shows that there are two pairs of well-defined hydrogen adsorption/desorption and metal oxidation/reduction peaks. From the hydrogen desorption region of Fig. 3a, the ECSA of CoPt TONPs is estimated to be 82.2 m^2 g^{-1}, much larger than that of CoPt ANPs (51.8 m^2 g^{-1}) and commercial Pt/C (63.1 m^2 g^{-1}), due to the relatively small size, unique structure and good dispersion. Large ECSA will enhance the catalytic performance, which is very important for the electrochemical activity of catalyst [38].

The electrocatalytic behaviors of these three samples toward MOR were evaluated by CVs in a mixed solution of 0.5 mol L^{-1} H_2SO_4 and 1 mol L^{-1} CH_3OH at a scan rate of 50 mV s^{-1}. As shown in Fig. 3b, the MOR curves have two well-separated peaks: the anodic peaks in the forward and backward scans. During the forward scan, the current density increases with increasing potential but then decreases with further increasing of potential, resulting in an obvious peak at around 0.7 V, which is attributed to the amount of methanol oxidized at the electrode surface [26,39]. When

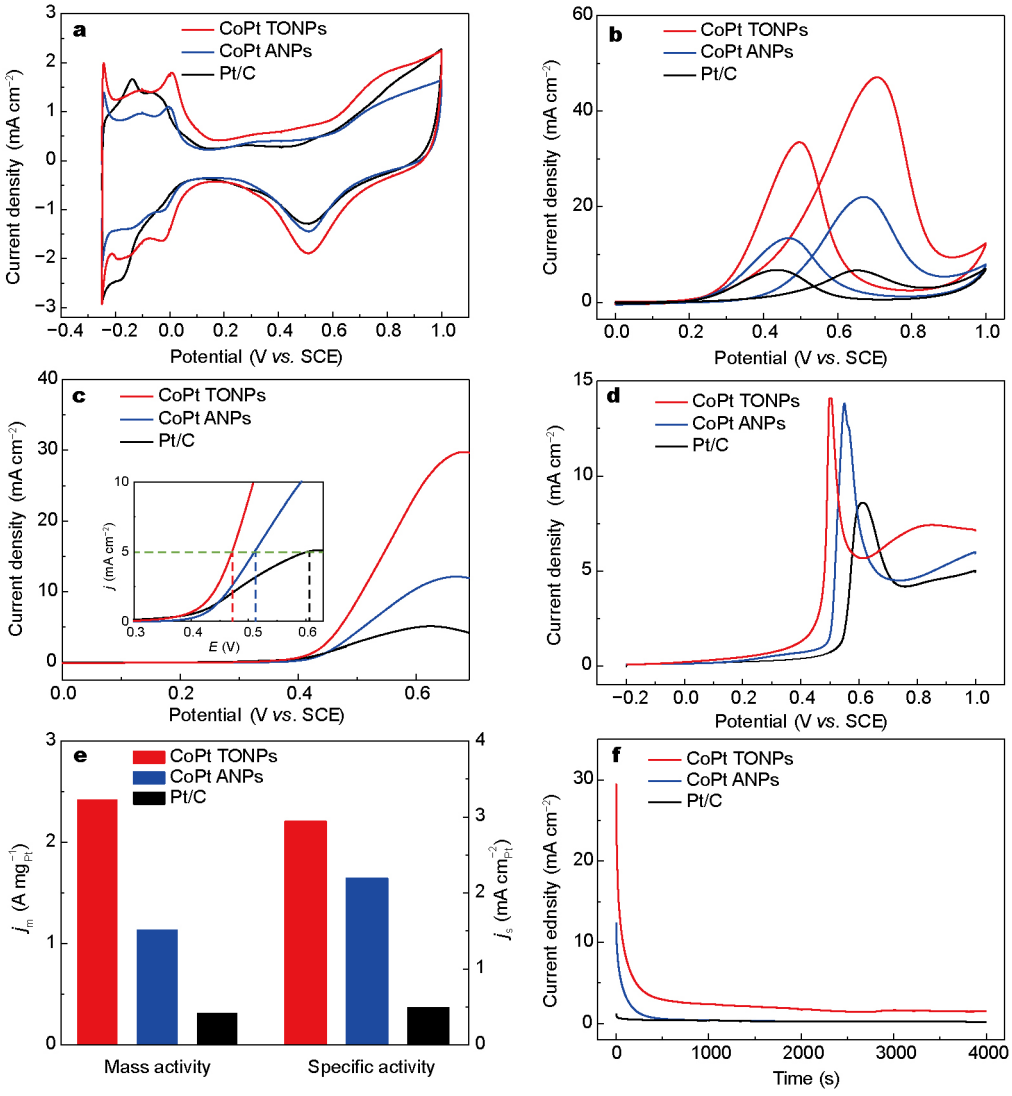

Figure 3 CV curves of CoPt TONPs, ANPs and commercial Pt/C in Ar-saturated 0.5 mol L^{-1} H_2SO_4 (a) and mixed with 1 mol L^{-1} CH_3OH solution at a scan rate of 50 mV s^{-1} (b); (c) LSV curves of various electrocatalysts in a mixed solution containing 0.5 mol L^{-1} H_2SO_4 and 1 mol L^{-1} CH_3OH with a low scan rate of 5 mV s^{-1}. Inset: enlarged view of the LSV curves; (d) CO stripping curves of CoPt TONPs, CoPt ANPs and commercial Pt/C in CO-saturated 0.5 mol L^{-1} H_2SO_4 solution at a scan rate of 50 mV s^{-1}; (e) mass and specific activities calculated from the forward oxidation current of (b); (f) chronoamperometry measured at 0.6 V *versus* SCE in a mixed solution of 0.5 mol L^{-1} H_2SO_4 + 1 mol L^{-1} CH_3OH at a scan rate of 50 mV s^{-1}.

the scan is backward, the oxidation peak at about 0.45 V is generated due to the oxidization of the residual carbon species [40]. From the MOR curves in Fig. 3b, the forward current density (j_f) of CoPt TONPs (47.1 mA cm^{-2}) is remarkably higher than that of CoPt ANPs (22.1 mA cm^{-2}) and commercial Pt/C (6.7 mA cm^{-2}), which is about 2 and 7 times that of CoPt ANPs and of commercial Pt/C, respectively.

Fig. 3c shows the LSV curves at a slow scan rate of 5 mV s^{-1} for the three catalysts in a mixed solution containing 0.5 mol L^{-1} H_2SO_4 and 1 mol L^{-1} CH_3OH. The peak current density of CoPt TONPs is 29.7 mA cm^{-2}, which is nearly 2.5 and 5.7 times that of CoPt ANPs (12.1 mA cm^{-2}) and commercial Pt/C (5.2 mA cm^{-2}), respectively. This is in good agreement with the CV results in Fig. 3b, further confirming that the CoPt TONPs possess the highest catalytic activity. Furthermore, the onset potentials for the three catalysts are strikingly different as well. For CoPt TONPs, it is nearly 20 mV lower than that of commercial Pt/C, implying clearly superior reaction kinetics together with higher efficiency to remove the incompletely oxidized carbonaceous species formed during the oxidation reaction, which will be discussed in the CO stripping results [41,42]. For example, if a certain oxidation current density is needed at 5 mA cm^{-2} (as displayed by the green dashed line in the inset of Fig. 3c), the corresponding oxidation potential on the CoPt ANPs (0.51 V) and Pt/C (0.61 V) are larger than that on CoPt TONPs (0.47 V). This relatively low trigger oxidation potential means that the MOR is much easier to carry out on CoPt TONPs [43].

CO stripping behavior was determined on the three electrocatalysts in CO-saturated 0.5 mol L^{-1} H_2SO_4 at a scan rate of 50 mV s^{-1}. As shown in Fig. 3d, the onset of CO stripping on CoPt TONPs (0.44 V) is lower than that on CoPt ANPs and standard commercial Pt/C, which are 0.50 and 0.54 V, respectively. Meanwhile, the corresponding CO oxidation peak of CoPt TONPs, CoPt ANPs and commercial Pt/C are also positively shifted from 0.50 to 0.61 V. These results suggest that the CoPt TONPs have the efficient CO removal ability, which might arise mainly from the optimum geometric, ligand effect between Co and Pt, which alters the electronic structure of Pt [26,44].

To further compare the electrocatalytic activities of the above three catalysts, loaded Pt mass-normalized forward peak current (mass activity) and the ECSA-normalized forward peak current (specific activity) at forward peak potential for MOR are summarized in Fig. 3e. The mass activity of CoPt TONPs is 2.4 A mg_{Pt}^{-1}, which is about 2 and 8 times that of CoPt ANPs (1.1 A mg_{Pt}^{-1}) and commercial Pt/C (0.3 A mg_{Pt}^{-1}), respectively. Moreover, the specific activity of CoPt TONPs is 2.9 mA cm_{Pt}^{-2}, which is greatly larger than that of CoPt ANPs (2.2 mA cm_{Pt}^{-2}) and commercial Pt/C (0.5 mA cm_{Pt}^{-2}). The better performance may originate from the modification of the electronic structure between Co and Pt together with the highest ESCA for more available catalytically active sites.

The electrocatalytic stability of the three samples were further characterized by chronoamperometry. The data shown in Fig. 3f were collected at a fixed potential of 0.6 V. Apparently, the current densities decrease rapidly for these three catalysts at the beginning, due to the formation of intermediate products such as CO_{ads}, $COOH_{ads}$ and CHO_{ads} [41]. However, much slower current density decay and higher oxidation current density are observed for CoPt TONPs compared with CoPt ANPs and commercial Pt/C.

Accelerated durability test (ADT) was also performed to further examine the stability of CoPt TONPs in comparison with CoPt ANPs and commercial Pt/C which were collected in an Ar-saturated 0.5 mol L^{-1} H_2SO_4 solution at a scan rate of 50 mV s^{-1}. After 1000 cycles, the CV curves used to calculate ECSA and the peak current density for the three catalysts are summarized in Figs 4, S5 and Table S1. As shown in Fig. 4d, the ESCA value shows a decrease because of the dissolution of surficial Pt atoms and agglomeration of Pt particles through surface oxidation/reduction processes. After ADT, the ECSA value of CoPt TONPs shown in Fig. 4a is 66.9 m^2 g^{-1}, which only decreases 18.5%, but it decreases as high as 31.7% and 68.2% for CoPt ANPs (remaining 35.4 m^2 g^{-1}) in Fig. 4b and commercial Pt/C (remaining 20.0 m^2 g^{-1}) in Fig. 4c, respectively. Fig. 4d shows the ECSA values of the three electrocatalysts before and after ADT. These results indicate that CoPt TONPs enhance long-term catalytic stability for MOR. The stable catalytic activity of CoPt TONPs indicates the improved ability to prevent CO poisoning, which can be attributed to the strong electron interaction between Co and Pt atoms in CoPt TONPs [26].

Based on the above experimental data, it is reasonable to conclude that the electrocatalytic activity and the stability of CoPt TONPs can be greatly enhanced. The reasons can be attributed to several facts. Frist, the ligand effect between Co and Pt can modify the electronic structure of Pt by the orbital overlap of 3d transition metal Co. As shown in Fig. 2d, the Pt 4f binding energy in CoPt TONPs shows a large shift which lowers Pt d-band center as well as the surface oxygen affinity [26,45]. Second, the addition of metal can also facilitate the generation of oxygen-containing species on sites adjacent to Pt, thereby aiding in the

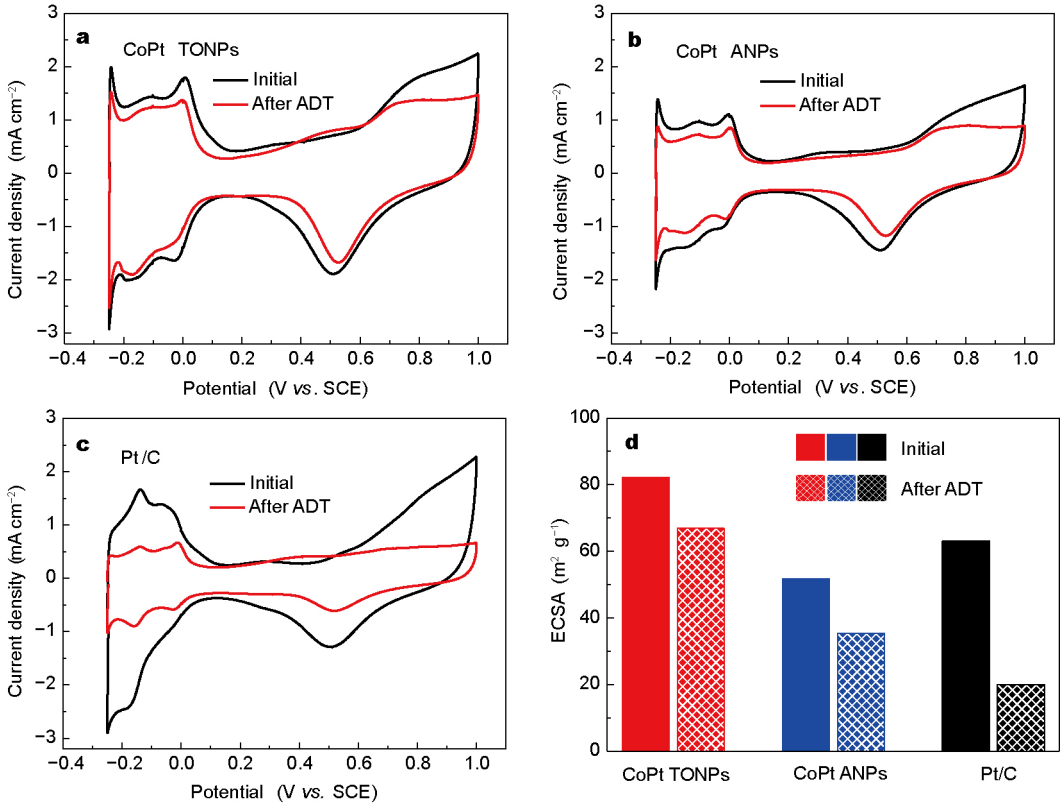

Figure 4 CV curves of CoPt TONPs (a), CoPt ANPs (b) and commercial Pt/C (c) before and after ADT collected in an Ar-saturated 0.5 mol L^{-1} H_2SO_4 solution at a scan rate of 50 mV s^{-1}; (d) the ECSA value of initial and after ADT for three electrocatalysts.

oxidation of CO and resulting in the great enhancement in electrocatalytic activities, which is called the bifunctional effect [41,45]. Third, the smaller size and better dispersion can enlarge surface area and are benifical for electron transfer to or from particle surface [46].

Pt as a universal choice of catalyst plays a dominant role in the elecrocatalytic performance. The introduction of magnetic elements (such as Co, Fe and Ni) not only dramatically decreases the usage of noble Pt, but also changes the structure of Pt to tune the electrocatalytic performance. Furthermore, the addition of Co will affect the magnetic property of bimetallic CoPt TONPs. Apparently, it is excellent for the catalysts to be recycled if they show ferromagnetism at RT. It is well known that the catalytic performance will be greatly enhanced if the reaction takes place at higher temperatures. At the same time, the magnetic materials will experience a magnetic transition with increasing temperature, such as from ferromagnetism to paramagnetism. Therefore, the relationship between catalytic and magnetic properties will be certainly amazing. Up to now, this is still an open issue due to its extremely complicated physical and chemical reactions. In this work, the magnetic measurements of the CoPt TONPs were carried out by SQUID and ESR. Fig. 5a shows the hysteresis loops (*M-H* loops) at 10, 200 and 300 K, where the inset presents the enlarged data. The coercivity (H_c) decreases with increasing temperature, and its value is 493, 116 and 15 Oe for 10, 200 and 300 K, respectively. Similarly, the saturation magnetization (M_s) shows a slight decrease with increasing temperature, such as 21 emu g^{-1} at 10 K and 16 emu g^{-1} at 300 K. It indicates that magnetic moments become more disorderly with increasing temperature, and will reach paramagnetism above Curie temperature [47,48]. The temperature dependent magnetization (*M-T* curves) for ZFC and FC are shown in Fig. 5b. The data show a typical ferromagnetic behavior and the Curie temperature is estimated to be above 350 K. Both the *M-H* loops and *M-T* curves confirm the ferromagnetism at RT for CoPt TONPs.

ESR spectroscopy is usually used to detect much weak ferromagnetism and paramagnetism, including metal-organic framework (MOF) [49]. Here, the magnetic property was further investigated by ESR highly sensitive detection under different temperatures, as shown in Fig. 5c. All the ESR curves possess the typical single Lorentz shape with

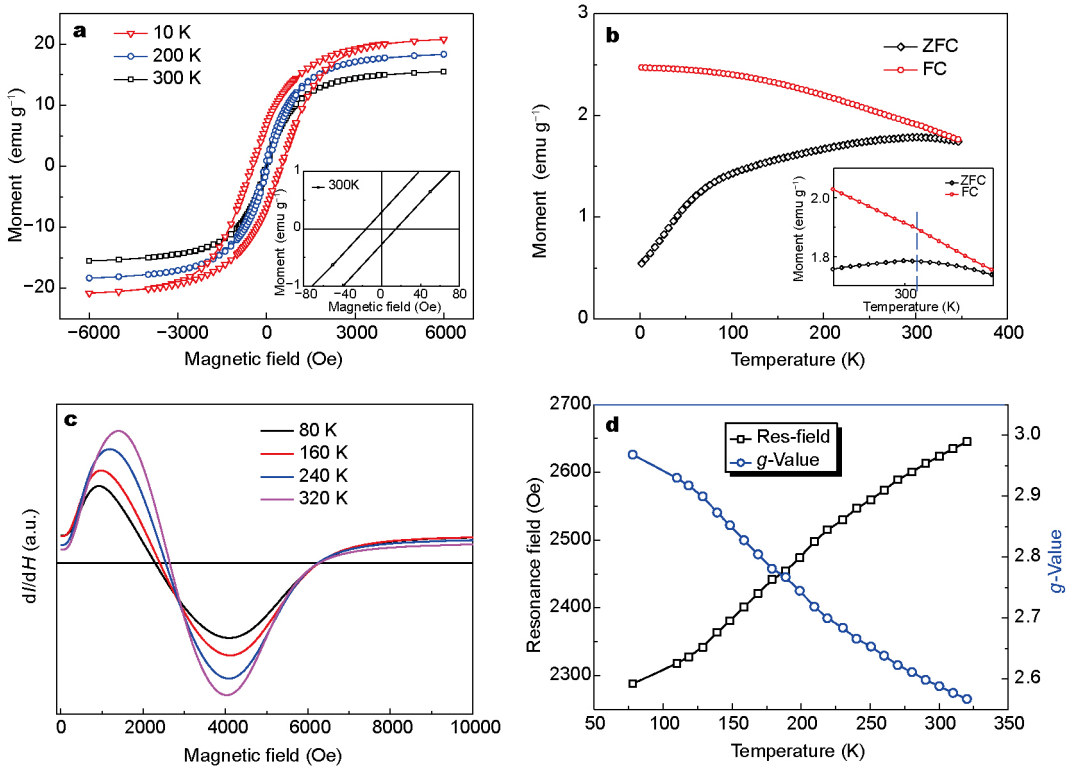

Figure 5 (a) *M-H* loops for CoPt TONPs at 10, 200 and 300 K, respectively; (b) ZFC and FC curves obtained with a magnetic field of 100 Oe; (c) ESR spectra at various temperatures; (d) corresponding resonance field and *g*-value.

good symmetry. The resonance field varies from 2288 to 2645 Oe with the temperature increasing from 80 to 320 K. The *g*-value can be calculated according to the following equation [50,51]:

$$h\nu = g\mu_B B_{res}, \quad (1)$$

where μ_B is the Bohr magneton, h is the Plank constant, and B_{res} is the resonance field obtained from the ESR curves, ν is the frequency of AC magnetic field, respectively. The resonance field and *g*-value as a function of temperature are presented in Fig. 5d. The *g*-value is nearly 2.0 for paramagnetism and increases for ferromagnetism. The value of *g* is larger than 2.0 for CoPt TONPs, confirming the ferromagnetism below 320 K. For example, the resonance field and *g*-value is 2474 Oe and 2.74 at 200 K, respectively. When the temperature is rised to 300 K, it changes to 2624 Oe with *g*-value of 2.59. The ferromagnetic signal becomes weaker with increasing temperature, well consistent with the SQUID results. The data from SQUID and the ESR provide a direct evidence for the ferromagnetism state in TONPs.

It is important to point out that the magnetic properties including Curie temperature, the coercivity can be changed by the structure, size, and shape of the NPs. Simultaneously, the catalytic behavior has a close connection with structure, size, shape, and steps on the surface. Therefore, there could be internal relationship between the magnetic and catalytic properties, especially in the micro/nano-scale particles. Based on the above results, we think the improvement of electrocatalyst might be associated with the magnetic properties. This may be a promising route to develop excellent electrocatalytic activity and stability with low Pt-loading on electrode in fuel cell by adding magnetic elements together with the control of structure, size, and shape.

CONCLUSIONS

In summary, CoPt TONPs were successfully produced by a simple and rapid one-pot method with great promising approach for the large scale production of electrocatalysts. The single crystalline CoPt TONPs can be as small as 8 nm with better electlocatalytic performance compared with CoPt ANPs and commercial Pt/C. The mass and specific activities of CoPt TONPs is 2.4 A mg_{Pt}^{-1} and 2.9 mA cm_{Pt}^{-2}, markedly higher than that of commercial Pt/C, which is only 0.3 A mg_{Pt}^{-1} and 0.5 mA cm_{Pt}^{-2}, respectively. After ADT, the ECSA value of the CoPt TONPs is about 3.3 times larger

than that of commercial Pt/C. In addition, the weak ferromagnetism at RT is quite useful for recycling the catalysts during industrial applications.

Received 11 October 2016; accepted 21 November 2016; published online 13 December 2016

1 Zhao X, Zhang J, Wang L, *et al.* Ultrathin PtPdCu nanowires fused porous architecture with 3D molecular accessibility: an active and durable platform for methanol oxidation. ACS Appl Mater Interfaces, 2015, 7: 26333–26339
2 Du X, Luo S, Du H, *et al.* Monodisperse and self-assembled Pt-Cu nanoparticles as an efficient electrocatalyst for the methanol oxidation reaction. J Mater Chem A, 2016, 4: 1579–1585
3 Liu H, Nosheen F, Wang X. Noble metal alloy complex nanostructures: controllable synthesis and their electrochemical property. Chem Soc Rev, 2015, 44: 3056–3078
4 Chung DY, Jun SW, Yoon G, *et al.* Highly durable and active PtFe nanocatalyst for electrochemical oxygen reduction reaction. J Am Chem Soc, 2015, 137: 15478–15485
5 Jung N, Bhattacharjee S, Gautam S, *et al.* Organic-inorganic hybrid PtCo nanoparticle with high electrocatalytic activity and durability for oxygen reduction. NPG Asia Mater, 2016, 8: e237
6 Stamenkovic VR, Fowler B, Mun BS, *et al.* Improved oxygen reduction activity on $Pt_3Ni(111)$ via increased surface site availability. Science, 2007, 315: 493–497
7 Huang W, Wang H, Zhou J, *et al.* Highly active and durable methanol oxidation electrocatalyst based on the synergy of platinum-nickel hydroxide-graphene. Nat Commun, 2015, 6: 10035
8 Vinayan BP, Ramaprabhu S. Platinum-TM (TM = Fe, Co) alloy nanoparticles dispersed nitrogen doped (reduced graphene oxide-multiwalled carbon nanotube) hybrid structure cathode electrocatalysts for high performance PEMFC applications. Nanoscale, 2013, 5: 5109–5118
9 Bu L, Ding J, Guo S, *et al.* A general method for multimetallic platinum alloy nanowires as highly active and stable oxygen reduction catalysts. Adv Mater, 2015, 27: 7204–7212
10 Xia BY, Wu HB, Li N, *et al.* One-pot synthesis of Pt-Co alloy nanowire assemblies with tunable composition and enhanced electrocatalytic properties. Angew Chem Int Ed, 2015, 54: 3797–3801
11 Mani P, Srivastava R, Strasser P. Dealloyed binary PtM_3 (M=Cu, Co, Ni) and ternary $PtNi_3M$ (M=Cu, Co, Fe, Cr) electrocatalysts for the oxygen reduction reaction: performance in polymer electrolyte membrane fuel cells. J Power Sources, 2011, 196: 666–673
12 Yang P, Jin SY, Xu QZ, *et al.* Decorating PtCo bimetallic alloy nanoparticles on graphene as sensors for glucose detection by catalyzing luminol chemiluminescence. Small, 2013, 9: 199–204
13 Xu Y, Yuan Y, Ma A, *et al.* Composition-tunable Pt-Co alloy nanoparticle networks: facile room-temperature synthesis and supportless electrocatalytic applications. Chem Phys Chem, 2012, 13: 2601–2609
14 Huang Y, Garcia M, Habib S, *et al.* Dealloyed PtCo hollow nanowires with ultrathin wall thicknesses and their catalytic durability for the oxygen reduction reaction. J Mater Chem A, 2014, 2: 16175–16180
15 Li C, Imura M, Yamauchi Y. Displacement plating of a mesoporous Pt skin onto Co nanochains in a low-concentration surfactant solution. Chem Eur J, 2014, 20: 3277–3282
16 Zhu J, Wu J, Liu F, *et al.* Controlled synthesis of FePt-Au hybrid nanoparticles triggered by reaction atmosphere and FePt seeds. Nanoscale, 2013, 5: 9141–9149
17 Yuan Q, Zhuang J, Wang X. Single-phase aqueous approach toward Pd sub-10 nm nanocubes and Pd-Pt heterostructured ultrathin nanowires. Chem Commun, 2009, 43: 6613
18 Cui C, Gan L, Heggen M, *et al.* Compositional segregation in shaped Pt alloy nanoparticles and their structural behaviour during electrocatalysis. Nat Mater, 2013, 12: 765–771
19 Yang T, Cao G, Huang Q, *et al.* Truncated octahedral platinum-nickel-iridium ternary electro-catalyst for oxygen reduction reaction. J Power Sources, 2015, 291: 201–208
20 Alam A, Kraczek B, Johnson DD. Structural, magnetic, and defect properties of Co-Pt-type magnetic-storage alloys: density-functional theory study of thermal processing effects. Phys Rev B, 2010, 82: 024435
21 Khemjeen Y, Pinitsoontorn S, Chompoosor A. Effect of boron addition on the structure and magnetic properties of CoPt nanoparticles. J Appl Phys, 2015, 117: 17D513
22 Saravanan P, Hsu JH, Tsai CL, *et al.* Interplay between out-of-plane anisotropic L11-type CoPt and in-plane anisotropic NiFe layers in CoPt/NiFe exchange springs. J Appl Phys, 2014, 115: 243905
23 Alloyeau D, Ricolleau C, Mottet C, *et al.* Size and shape effects on the order-disorder phase transition in CoPt nanoparticles. Nat Mater, 2009, 8: 940–946
24 Liu J, Xia T, Wang S, *et al.* Oriented-assembly of hollow FePt nanochains with tunable catalytic and magnetic properties. Nanoscale, 2016, 8: 11432–11440
25 Yu Y, Yang W, Sun X, *et al.* Monodisperse MPt (M = Fe, Co, Ni, Cu, Zn) nanoparticles prepared from a facile oleylamine reduction of metal salts. Nano Lett, 2014, 14: 2778–2782
26 Zheng JN, He LL, Chen C, *et al.* One-pot synthesis of platinum$_3$cobalt nanoflowers with enhanced oxygen reduction and methanol oxidation. J Power Sources, 2014, 268: 744–751
27 Xu J, Liu X, Chen Y, *et al.* Platinum-cobalt alloy networks for methanol oxidation electrocatalysis. J Mater Chem, 2012, 22: 23659–23667
28 Tseng YC, Chen HS, Liu CW, *et al.* The effect of alloying on the oxygen reduction reaction activity of carbon-supported PtCu and PtPd nanorods. J Mater Chem A, 2014, 2: 4270–4275
29 Wagner CD, Muilenberg GE. Handbook of X-ray Photo-Electron Spectroscopy. Minnesota: Perkin-Elmer Corporation, 1979
30 Sun X, Jiang K, Zhang N, *et al.* Crystalline control of {111} bounded Pt_3Cu nanocrystals: multiply-twinned Pt_3Cu icosahedra with enhanced electrocatalytic properties. ACS Nano, 2015, 9: 7634–7640
31 Chen C, Kang Y, Huo Z, *et al.* Highly crystalline multimetallic nanoframes with three-dimensional electrocatalytic surfaces. Science, 2014, 343: 1339–1343
32 Xia T, Liu J, Wang S, *et al.* Enhanced catalytic activities of NiPt truncated octahedral nanoparticles toward ethylene glycol oxidation and oxygen reduction in alkaline electrolyte. ACS Appl Mater Interfaces, 2016, 8: 10841–10849
33 Tan XH, Prabhudev S, Kohandehghan A, *et al.* Pt-Au-Co alloy electrocatalysts demonstrating enhanced activity and durability toward the oxygen reduction reaction. ACS Catal, 2015, 5: 1513–1524
34 Cui C, Gan L, Li HH, *et al.* Octahedral PtNi nanoparticle catalysts: exceptional oxygen reduction activity by tuning the alloy particle surface composition. Nano Lett, 2012, 12: 5885–5889
35 Dai L, Zhao Y, Chi Q, *et al.* Morphological control and evolution of octahedral and truncated trisoctahedral Pt-Au alloy nanocrystals under microwave irradiation. Nanoscale, 2014, 6: 9944–9950
36 Fu QQ, Li HH, Ma SY, *et al.* A mixed-solvent route to unique PtAuCu ternary nanotubes templated from Cu nanowires as efficient dual electrocatalysts. Sci China Mater, 2016, 59: 112–121
37 Shan A, Chen Z, Li B, *et al.* Monodispersed, ultrathin NiPt hollow

nanospheres with tunable diameter and composition via a green chemical synthesis. J Mater Chem A, 2015, 3: 1031–1036
38 Fu S, Zhu C, Shi Q, *et al.* Highly branched PtCu bimetallic alloy nanodendrites with superior electrocatalytic activities for oxygen reduction reactions. Nanoscale, 2016, 8: 5076–5081
39 Hu C, Han Q, Zhao F, *et al.* Graphitic C_3N_4-Pt nanohybrids supported on a graphene network for highly efficient methanol oxidation. Sci China Mater, 2015, 58: 21–27
40 Wang S, Yang G, Yang S. Pt-frame@Ni *quasi* core-shell concave octahedral $PtNi_3$ bimetallic nanocrystals for electrocatalytic methanol oxidation and hydrogen evolution. J Phys Chem C, 2015, 119: 27938–27945
41 Wang DY, Chou HL, Lin YC, *et al.* Simple replacement reaction for the preparation of ternary $Fe_{1-x}PtRu_x$ nanocrystals with superior catalytic activity in methanol oxidation reaction. J Am Chem Soc, 2012, 134: 10011–10020
42 Liu H, Adzic RR, Wong SS. Multifunctional ultrathin $Pd_xCu_{1-x}$and Pt~Pd_xCu_{1-x} one-dimensional nanowire motifs for various small molecule oxidation reactions. ACS Appl Mater Interfaces, 2015, 7: 26145–26157
43 Lai S, Fu C, Chen Y, *et al.* Pt-content-controlled synthesis of Pd nanohollows/Pt nanorods core/shell composites with enhanced electrocatalytic activities for the methanol oxidation reaction. J Power Sources, 2015, 274: 604–610
44 Chen Q, Zhang J, Jia Y, *et al.* Wet chemical synthesis of intermetallic Pt_3Zn nanocrystals via weak reduction reaction together with UPD process and their excellent electrocatalytic performances. Nanoscale, 2014, 6: 7019–7024
45 Cai Z, Kuang Y, Qi X, *et al.* Ultrathin branched PtFe and PtRuFe nanodendrites with enhanced electrocatalytic activity. J Mater Chem A, 2015, 3: 1182–1187
46 Zhao ZL, Zhang LY, Bao SJ, *et al.* One-pot synthesis of small and uniform Au@PtCu core-alloy shell nanoparticles as an efficient electrocatalyst for direct methanol fuel cells. Appl Catal B-Environ, 2015, 174-175: 361–366
47 Shan A, Liu W, Wang R, *et al.* Magnetism in undoped ZnS nanotetrapods. Phys Chem Chem Phys, 2013, 15: 2405–2410
48 Sun Q, Wang S, Wang R. Well-aligned CoPt hollow nanochains synthesized in water at room temperature. J Phys Chem C, 2012, 116: 5352–5357
49 Wang W, Yan LQ, Cong JZ, *et al.* Magnetoelectric coupling in the paramagnetic state of a metal-organic framework. Sci Rep, 2013, 3: 2024
50 Shaw JM, Nembach HT, Silva TJ, *et al.* Precise determination of the spectroscopic *g*-factor by use of broadband ferromagnetic resonance spectroscopya. J Appl Phys, 2013, 114: 243906
51 Ulmeanu M, Antoniak C, Wiedwald U, *et al.* Composition-dependent ratio of orbital-to-spin magnetic moment in structurally disordered Fe_xPt_{1-x} nanoparticles. Phys Rev B, 2004, 69: 054417

Acknowledgments This work was supported by the National Basic Research Program of China (2015CB921401), the National Instrument Program of China (2012YQ120048), the National Natural Science Foundation of China (51625101, 51431009, 51471183, 51331002, 51371015, 11274371 and 11674023), the Instrument Development Program of Chinese Academy of Sciences (YZ201345), and the Fundamental Research Funds for the Central Universities (FRF-BR-15-009B).

Author contributions Xia T designed and performed the experiments, analyzed the data and wrote the paper; Wang S and Wang R analyzed the results and put forward valuable suggestions; Liu J, Wang C and Sun Y helped with the experiments; All authors contributed to the general discussion.

Conflict of interest The authors declare that they have no conflict of interest.

Supplementary information Supplementary data are available in the online version of the paper.

Tianyu Xia received her master degree from the Capital Normal University in 2013. She is now a PhD student supervised by Prof. Shouguo Wang and Rongming Wang in Beihang University. Her current research is focused on the synthesis and characterization of noble nanomaterials.

Shouguo Wang received his bachelor degree (1996) from Anhui University and PhD (2001) from the Institute of Solid State Physics, Chinese Academy of Sciences (CAS), respectively. From August 2001 to December 2007, he did his research at the National University of Singapore, Max-Planck-Institute of Microstructure Physics, and the Univerity of Oxford. At the end of 2007, he joined the State Key Laboratory of Magnetism, Institute of Physics-CAS. He moved to the School of Materials Science and Engineering, University of Science and Technology Beijing in January 2016. His research interests include the magnetism and magnetic materials, with a focus on the topological magnetism such as skyrmions, spintronics, and nanomagnetism.

Rongming Wang received his bachelor (1991) and master's (1994) degrees in physics from Peking University and PhD (1997) in materials science from Beijing Institute of Aeronautical Materials (BIAM), China. He joined Peking University as an associate professor in 2002. He joined Beihang University as a professor of physics in 2005 and joined the University of Science and Technology Beijing in 2015. His research interests include the synthesis, atomic structure and properties of functional nanomaterials. He has co-authored over 160 peer reviewed papers and has a research H-index of 39.

室温铁磁性CoPt纳米截角八面体的简易合成及超高电催化特性表征

夏田雨[1,2,3], 刘家龙[2], 王守国[1,3*], 王超[3], 孙阳[3], 王荣明[1,2*]

摘要 本文通过简单的一步法成功制备出室温铁磁性CoPt纳米截角八面体. 这种平均大小约为8 nm的单晶CoPt截角八面体纳米结构在催化甲醇氧化反应时表现出优异的电催化活性及稳定性, 其质量活性和相对比活性分别能够达到标准商业Pt/C催化剂的8倍及6倍. 长时间加速稳定性测试结果表明, CoPt纳米截角八面体的电化学活性表面积仅损失了18.5%, 而相同反应条件下的标准商业Pt/C电极却损失了68.2%. 磁性分析发现, 这些仅有8 nm大小的CoPt纳米截角八面体的居里温度高达350 K, 并在室温下表现出较弱的铁磁性, 这将更加有利于催化剂的回收再利用, 在实际应用中具有较大的潜在价值.